THE PERFORMANCE OF A NEW IMMERSED BOUNDARY METHOD ON SIMULATING UNDERWATER LOCOMOTION AND SWIMMING

Arman Hemmati[1], **Utku Şentürk**[2], **Tyler Van Buren**[3], **Alexander J. Smits**[4]
[1,3,4]Department of Mechanical and Aerospace Engineering, Princeton University, NJ, USA
[2]Department of Mechanical Engineering, Ege University, Turkey
[4]Department of Mechanical and Aerospace Engineering, Monash University, VIC, Australia

[1]ahemmati@princeton.edu, [2]utku.senturk@ege.edu.tr, [3]tburen@princeton.edu, [4]asmits@princeton.edu

ABSTRACT

We report the benchmark results of a new Immersed Boundary Method (IBM) incorporated into Direct Numerical Simulation (DNS) of a pitching panel, representing fish-like swimming, using *foam-extend-3.2*. The panel is flat and thin, and it has a triangular (convex) trailing edge, similar to that seen in the caudal fin of some fish. The accuracy of the solver is verified by comparing four cases of bluff body wake simulations with reported experimental and numerical studies. For example, the structure of the mean wake compared well with that obtained using PIV in a companion experiment. The differences in thrust generation and propulsion efficiency of square and convex thin panels are examined to identify the effect of trailing edge shape using proper orthogonal decomposition. The effect of Reynolds number is also evaluated by comparing the wake at Reynolds numbers of 2,000 and 10,000.

INTRODUCTION

Many biological species have evolved to develop efficient propulsive systems for swimming that also exhibit high speed and maneuverability (Sambiley, 1990; Sumich & Morrissey, 2004). Understanding the mechanics of aquatic propulsion has attracted the attention of many researchers over the years. Such explorations can yield valuable information on designing energy efficient and fast systems with high maneuverability and stealth that match and possibly surpass the performance of biological species. In this regard, it is often useful to focus on simple systems that can be used to study fundamental aspects of swimming performance. For instance, the implications of the trailing-edge shape of a tail fin as well as its orientation and movement (that is, harmonic fin motion) on the formation of vortex structures, wake dynamics and thrust generation plays a dominant role in understanding physics of fish-like swimming (Van Buren *et al.*, 2016).

The oscillating motion of a NACA 0012 airfoil was studied by Triantafyllou *et al.* (1991) as a representative of swimming motion by fish, which demonstrated a maximum propulsive efficiency of 25% for the Strouhal number $St = 0.25 - 0.35$, where $St = f_p c/U$, f_p is the frequency of oscillation, c is the fin characteristic length, and U is the swimming speed. The extensive study by Buchholz & Smits (2006) on the wake of a pitching rigid rectangular panel at moderate Reynolds numbers ($Re = Uc/\nu$) revealed that the flow is dominated by horseshoe-like structures. The aspect ratio of the panel was identified to impact the wake, and thus, the propulsive performance efficiency, which ranged from $9\% - 21\%$. Green & Smits (2008) investigated the distribution of pressure on the pitching panel, which revealed that the favorable streamwise pressure gradient that is present over most of the panel reversed near the trailing edge. There are many experimental challenges, however, in determining detailed surface pressure distributions in unsteady wakes, and it is even more difficult to determine the instantaneous shear stress distributions. In contrast, computational fluid dynamics (CFD) can be used to give insight into the stress distributions, and characterize the wake and identify implications of the wake dynamics on thrust generation. CFD simulations can also be helpful in providing insight into wake structures, their formation and interactions, and the effects of Reynolds number.

Numerical simulations of Blondeaux *et al.* (2005) on a pitching foil showed vortex-loop (chain-like) structures dominate the wake at $Re = 1000$, as found experimentally by Green *et al.* (2011). Blondeaux *et al.* (2005) used a distinctly developed CFD solver based on the Immersed Boundary Method (IBM). Jantzen *et al.* (2014) also used an IBM-based CFD solver to evaluate the wake of pitching rigid rectangular panels at $Re = 300$. This study provided details on the vortex formation process in the wake of rectangular panels of aspect ratios 2 and 4, revealing that the Reynolds number influences the formation frequency and length of leading edge vortices, and that higher aspect ratios result in early detachment of leading edge vortices.

The IBM is routinely used in fluid flow simulations as an alternative to the boundary-fitted method due to its lower computational cost. The IBM formulation in *foam-extend-3.2* uses a discrete forcing approach based on a weighted least square approximation to impose boundary conditions independent of the actual boundaries. This approach can capture the boundary as a sharp interface, which eliminates the issue of smearing. It also mitigates the distortion of cells around the moving boundaries, while alleviating errors that arise from transformation of curvilinear grids (Lundquist *et al.*, 2009). See also Iaccarino & Verzicco (2003) and Mittal & Iaccarino (2005).

Jasak *et al.* (2014) incorporated the IBM forcing approach into OpenFOAM as part of *foam-extend-3.2*. Case studies included flows over fixed bodies. In particular, a high Re flow case using the $k - \varepsilon$ model showed a lack of stability for extreme mesh refinements. Şentürk *et al.* (2016) extended this work to consider the (a) 2D flow over a stationary circular cylinder, (b) 2D wake of a transversely

oscillating cylinder, (c) 3D wake of a stationary flat plate of aspect ratio 1.0, and (d) 3D wake of a pitching flat plate of aspect ratio 1.0. The accuracy of this solver was evaluated by comparing the results of these cases against those of available experimental and numerical studies, and the results showed generally very good agreement.

The current study further extends to provide a more comprehensive description of the IBM tools incorporated in *foam-extend-3.2*, and then uses the computations to study the physics of the harmonic motion of two panels: a square flat panel, and one with a triangular trailing-edge (TE) with a trailing-edge corner angle of 135°. These two cases were chosen because of the observation by Van Buren *et al.* (2016) that the triangular TE panel displayed higher efficiency and larger thrust generation than the square panel under similar conditions. Specifically, it examines the effect of Reynolds number and the shape of trailing edge on wake structures and propulsive performance of the panel, while evaluating the orientation and shape of dominant 3D structures in the wake.

PROBLEM DESCRIPTION

The problem considered here is the flow over a flat, thin panel that pitches sinusoidally about its leading edge. Two panels are considered: a square panel measuring $c \times c$, and a panel with a triangular trailing edge but the same surface area (see Figure 1). The 3D incompressible Navier-Stokes (Eq. 3) and the continuity (Eq. 2) equations,

$$\frac{\partial u_i}{\partial t} + u_j \frac{\partial u_i}{\partial x_j} = -\frac{1}{\rho}\frac{\partial p}{\partial x_i} + \nu \frac{\partial^2 u_i}{\partial x_j x_j} \tag{1}$$

$$\frac{\partial u_i}{\partial x_i} = 0, \tag{2}$$

were solved using Direct Numerical Simulations (DNS) and IBM, where u is the velocity tensor, t is time, ρ is fluid density, ν is fluid kinematic viscosity, and x is the spatial coordinate identifier. The variables presented in this paper are normalized by the panel span (c) and the inlet uniform velocity (U_∞). The wake at Re =2000 and 10,000 were evaluated to investigate the effect of Reynolds number. Experimental results on these flow cases were obtained by Van Buren *et al.* (2016) at $Re = 6000$.

The computational domain (Figure 1) was designed following Taira & Colonius (2009) and Jantzen *et al.* (2014). Details of the numerical simulations (i.e., domain size, boundary conditions, etc.) can be found in Şentürk *et al.* (2016). The 3D cartesian coordinate system was used with the origin located at the panel geometrical center. The computational domain size was $[8,5,5]$ in the $[x,y,z]$ directions, respectively, where x aligns with the streamwise (direction of the flow), y with the spanwise, and z with the chordwise directions. The inlet was located $2c$ upstream of a pitching rigid panel. All side boundaries were separated by $2.5c$ from the panel centroid. The panel was set to oscillate freely about the $z-$axis (Figure 1),

$$\theta(t) = \theta_{max} sin(2\pi f_p t) \tag{3}$$

where θ is the pitch angle (Figure 1), θ_{max} is the maximum pitch angle set at 8°, and $f_p = 0.718$ is the pitching frequency. The symmetric triangular trailing edge shape of the convex panel represent pointed-tail fish type based on the panel trailing edge corner angle of 135° shown in Figure 1.

The uniform flow condition was enforced on the inlet boundary, where $u = U_\infty, v = w = 0$ and $\partial p/\partial n = 0$. The Neumann outflow condition ($\partial u/\partial n = \partial p/\partial n = 0$) was assigned to the outlet boundary. All side boundary conditions were set as slip condition with $\partial u/\partial \tau = 0$, $u.n = 0$, and $\partial p/\partial n = 0$. The slip condition was also imposed on the panel surfaces. The panel thickness of one spatial grid element constituted the case of a zero-thickness flat panel.

A total of 3.24 million hexahedral elements were used for the non-homogeneous spatial grid distribution. The smaller elements were concentrated around the panel and its immediate wake and larger elements formed at the boundaries. The temporal grid was uniform with a fixed timestep resulting in a maximum Courant number of 0.5. The pressure and velocity tolerance of 10^{-6} was set as the convergence criterion using a combined pressure-implicit split-operator (PISO) and semi-implicit method for pressure-linked equations (SIMPLE) algorithms which is referred to as PIMPLE.

The *foam-extend-3.2*, which is an extension to OpenFOAM, was used to carry out these simulations. The capabilities of this finite-volume solver to work with unstructured, collocated and body-fitted grids make it suitable for a wide range of large-scale industrial problems. The recent implementation of IBM capabilities to *foam-extend-3.2*, which was achieved without significant alternations to structure of the existing code, has made it attractive for problems with a moving mesh (Blondeaux *et al.*, 2005; Jantzen *et al.*, 2014; Şentürk *et al.*, 2016). More detailed discussion of the discretization methods can be found in Jasak (1996) and Tuković & Jasak (2012).

A background grid and an immersed boundary (IB) surface are required for the IB solvers. The latter was introduced as an STL (STereoLithography) file that triangulates the IB grid data and perform dot product procedures between the normal of its triangular and background grid cell centers through a loop on the IB surface. Thus, the cells inside the IB surface were tagged as solid cells and did not contribute to the solution, whereas faces that were not mutual between a solid and a non-solid cell were marked as IB cells and constituted the discitized domain. The boundary

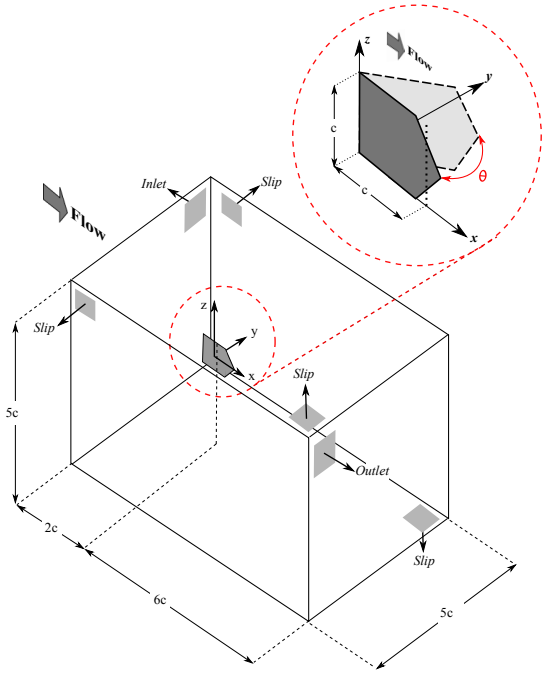

Figure 1: Computational domain (not to scale).

conditions were enforced on the IB surface using a weighted least square interpolation to assign appropriate values to variables in IB cells. Thus, the interpolation of any variable (φ) was carried out by minimizing $\sum_{i=1}^{n} w_i(\varphi_i - \tilde{\varphi}_i)^2$ for n number of cells. The unknown coefficients for the interpolation of $\tilde{\varphi}_i$ were determined using $\mathbf{C} = (\mathbf{M}^T\mathbf{W}\mathbf{A})^{-1}\mathbf{M}^T\mathbf{W}\mathbf{A}$, where components of $\mathbf{A}$ were defined in terms of $\tilde{\varphi}$, where $\mathbf{W}$ is the weight matrix and $\mathbf{M}$ is the design matrix. Thus, the elements of matrices $\mathbf{A}$, $\mathbf{M}$, and $\mathbf{W}$ differ based on the assigned boundary condition. For example, in case of the Dirichlet velocity boundary condition, φ is defined as

$$\tilde{\varphi}_i = \tilde{\varphi}_{ibp} + C_0 X_i + C_1 Y_i + C_2 X_i Y_i + C_3 X_i^2 + C_4 Y_i^2, \quad (4)$$

where $\tilde{\varphi}_{ibp}$ represents the point on IB surface closest to the ith cell and C is the unknown coefficient. Thus, elements of $\mathbf{A}$ are of the type $\tilde{\varphi}_i - \tilde{\varphi}_{ibp}$, and $\mathbf{M}$ is built solely on the geometric information. The corresponding weights on matrix $\mathbf{W}$ are defined as

$$w_{ii} = \frac{1}{2}\left[1 + cos\left(\pi \frac{r_i}{Sr_{max}}\right)\right], \quad (5)$$

where r is the distance between the interpolation cell and the nearest IB cell, and S is a tweaking parameter that prevents the exclusion of the furthest interpolation cell.

RESULTS & DISCUSSION

We begin by identifying the main structures and characteristics of the wake for the two panels considered here (square and triangular trailing edge) at $Re = 10,000$ to evaluate the effect of trailing edge shape. This discussion is followed by a more detailed analysis of the wake at $Re = 2000$ and $10,000$ along with comparison to experimental results of Van Buren *et al.* (2016) at $Re = 6000$.

Effect of Trailing Edge

The wake of a square panel is dominated by chain-like structures as shown in Figure 2, which is consistent with the wake model hypothesized by Buchholz & Smits (2006) and the numerical results of Şentürk & Smits (2016). The contours of the vorticity components normal to the surface in Figure 2a identified the vortex breakdown at only $x^+ \approx 2.2$ (where $x^+ = x/c$) downstream of the trailing edge. The trailing-edge vortex formed at the advancing face of the panel during the down-stroke motion (T_1), and it included a region of fluid with opposite vorticity at its core. A similar behavior was observed for S_1, which is the previously detached structure from the trailing edge relative to T_1. The structures broke down at $x^+ \approx 2.2$, as is apparent by the shape of S_2 and S_3. Furthermore, compressed vortex pairs (i.e., VP_3 compared to VP_1 and VP_2) shown in Figure 2b demonstrate the vortex interactions and breakdown of structures in the wake. These observation are in complete agreement with the findings of Buchholz & Smits (2006) and Şentürk & Smits (2016).

The formation of vortices on leading edge of the triangular trailing edge (convex) panel (L_3 and L_4 in Figure 3a) were similar to that seen for the square panel (L_1 and L_2 in Figure 2a). However, structures in the wake of the convex panel (Figure 3a) exhibited no sign of breakdown. Moreover, the vortex connections remained intact further downstream in the wake and there was evidence for the presence of vortex pairs at $x^+ \geq 3$, in contrast to that seen for the square panel (Figure 2a). Vortex pairs shown in Figure 3b underwent more severe spanwise negative-straining (vortex compression) relative to the square panel. Thus, one can argue that smaller vortex distortion on the plane of oscillation along with larger distortion on the plane parallel to the axis of oscillation results in higher propulsive performance (efficiency) and faster swimming (larger thrust).

The wake evolution for the two panel types are compared in Figure 4, in which the iso-surface of λ_2 criterion is presented at $Re = 10,000$. Here, λ_2 is defined as the second eigenvalue of $S_{ik}S_{kj} + \Omega_{ik}\Omega_{kj}$, where S_{ij} is the strain rate and Ω_{ij} is the rotation rate tensor (Jeong & Hussain, 1995). The chain-like vortex structures dominate the wake for both panels (Figure 4). The wake of the square panel (Figure 4a)

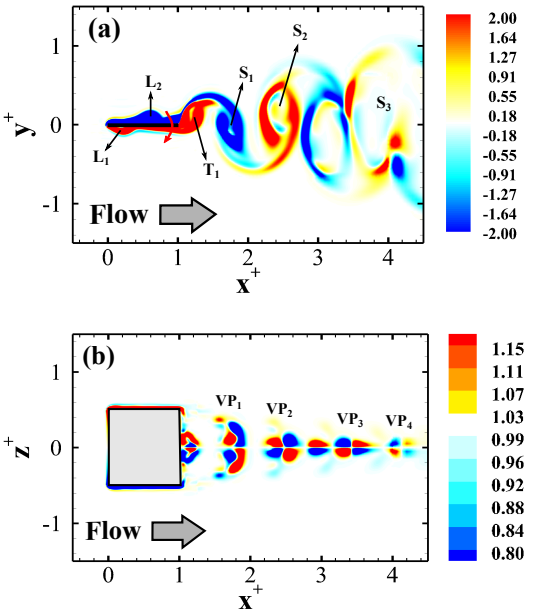

Figure 2: Contours of (a) chordwise vorticity (ω_z) and (b) spanwise vorticity (ω_y) for the square panel at $Re = 10,000$.

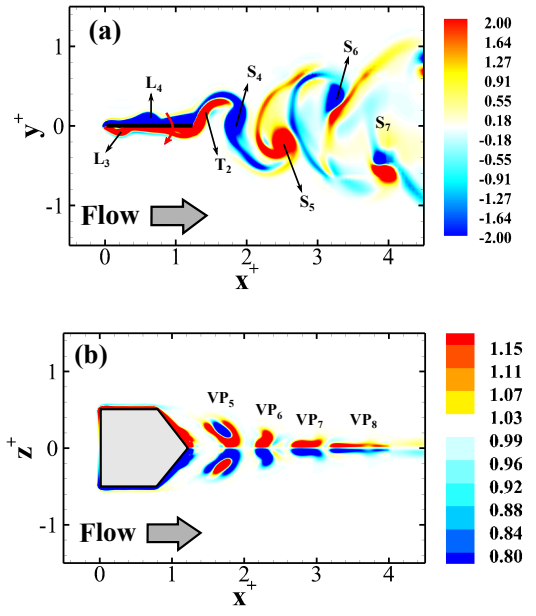

Figure 3: Contours of (a) spanwise vorticity (ω_z) and (b) chordwise vorticity (ω_y) for the convex panel at $Re = 10,000$.

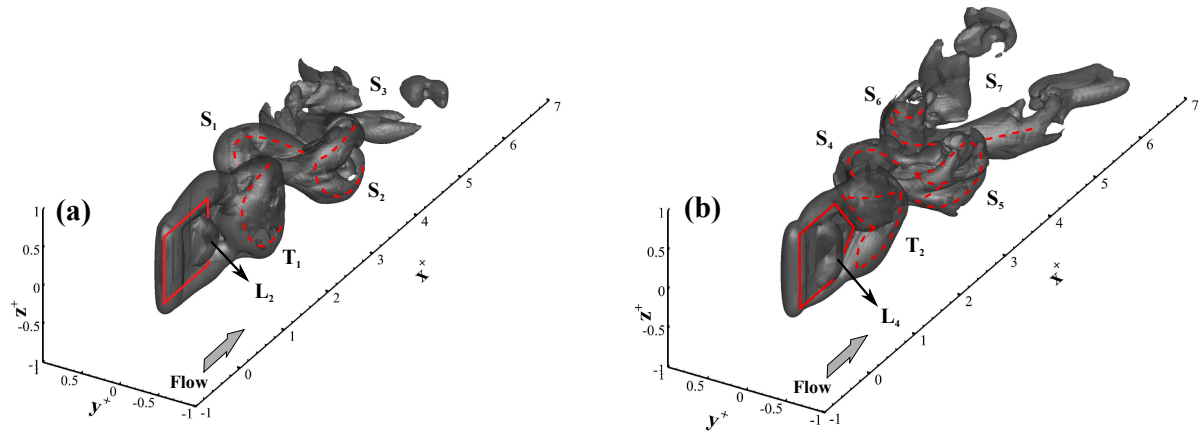

Figure 4: Isosurface plot of $\lambda_2 = -1.5$ for (a) square and (b) convex panels at $Re = 10,000$.

diffused more quickly compared to that of the convex panel (Figure 4b). Wake structures for the latter appeared more strained than the former with the wake experiencing a split at the centerline (S_7 in Figure 4b compared to S_3 in Figure 4a). The trailing-edge-vortex for the convex panel (T_2 in Figure 4b) retained the shape of the trailing edge, which remained unchanged despite severe straining in the wake.

Effect of Reynolds Number

Şentürk & Smits (2016), using a similar computational study, showed that the wake for the pitching square panel appeared to become Reynolds number independent at $6000 \lessapprox Re \lessapprox 8000$. In the current study, the wake of the convex panel is examined at $Re = 2000$ and $10,000$. Contours of time-averaged velocity magnitude ($|\overline{u^\star}|$) on $xy-$ and $xz-$planes are compared for the two Reynolds numbers in Figures 5 and 6. Figures 5a and 6a show a significant reduction of the base vortex size at higher Reynolds numbers; the length of the recirculation region shortens by a factor of about c as the Reynolds number increases by a factor of 5. The larger fluid velocity at the panel leading edges at the higher Reynolds number was accompanied with a smaller width of the wake in the spanwise (y) direction.

The effects of Reynolds number on time-averaged characteristics of the wake are more significant on the chordwise ($xz-$) plane (Figures 5b and 6b). The base vortex is significantly smaller and narrower for the higher Reynolds number, while the flow velocity in the region connecting the panel to the base vortex is significantly larger. In addition, the volume of low velocity flow formed at the leading edge reduces downstream at a slower rate at higher Reynolds numbers, which is apparent with the smaller region of low velocity flow on the panel surface (Figures 6b and 5b).

The coefficient of thrust generated by the convex pitching panel was $+0.021$ at $Re = 10,000$, while it was -0.0031 at $Re = 2000$. Thus, the smaller wake and the restriction of low velocity fluid to the vicinity of the leading edge at higher Reynolds number assisted in increasing thrust by minimizing drag on the panel surfaces. Moreover, the higher propulsive efficiency at $Re = 10,000$ relative to 2000 was attributed to the smaller wake and lower drag. The iso-

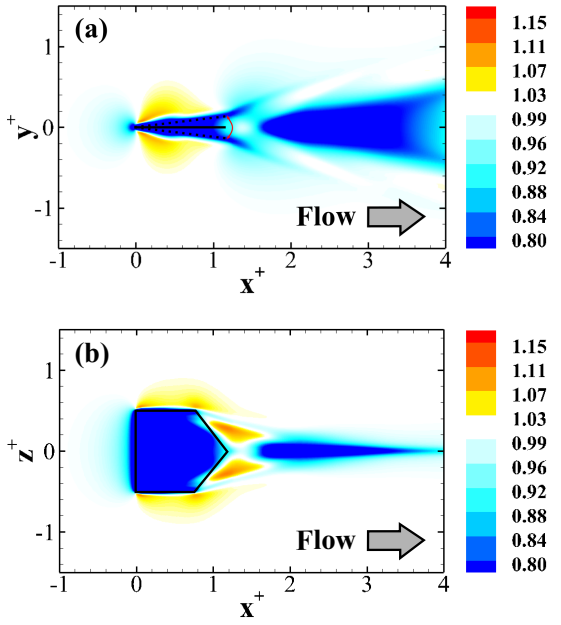

Figure 5: Contour of time-averaged velocity magnitude ($|\overline{u^\star}|$) on the $xy-$ (a) and $xz-$ (b) planes for $Re = 2000$.

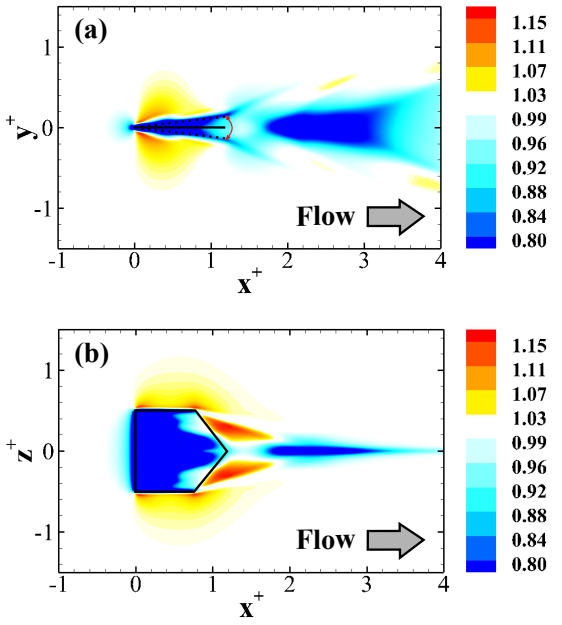

Figure 6: Contour of time-averaged velocity magnitude ($|\overline{u^\star}|$) on the $xy-$ (a) and $xz-$ (b) planes for $Re = 10,000$.

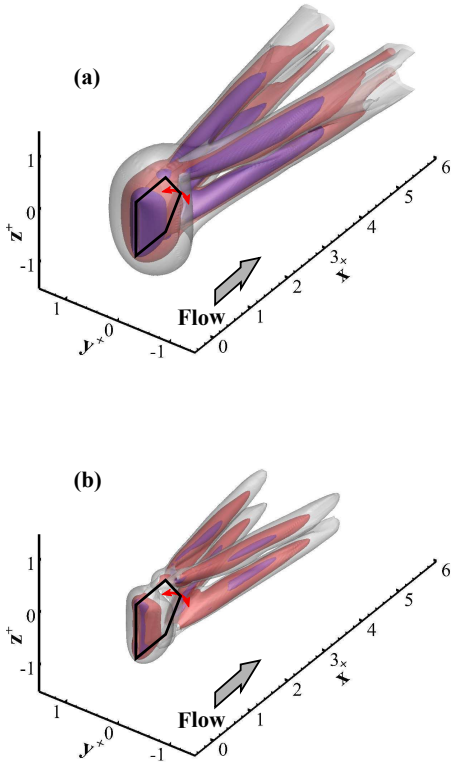

Figure 7: Iso-surface of $|\overline{u^\star}| = 1.01$ (gray), 1.02 (red) and 1.04 (blue) for a thin convex panel at (a) $Re = 2000$ and (b) 10,000.

surfaces of time-averaged velocity magnitude for the two cases in Figure 7 provide further evidence of the smaller time-average wake (compare the iso-surface of $|\overline{u^\star}| = 1.01$ at $Re = 10,000$ in Figure 7b with $Re = 2000$ in Figure 7a). Also, the region of higher velocity (say, $|\overline{u^\star}| = 1.04$) indicates that there are lower velocity gradients in the base region at higher Reynolds number. Moreover, the shape of the trailing edge of the convex panel resulted in a four-branched base vortex compared to the square panel (Şentürk & Smits, 2016; Van Buren *et al.*, 2016), which may be associated with higher thrust and efficiency.

The iso-surface plot of the time-averaged streamwise velocity ($\overline{u^\star}$) obtained by the DNS at two Reynolds numbers are compared against experimental (PIV) results of Van Buren *et al.* (2016) at $Re = 6000$ in Figure 8. The mean wake for the DNS and the PIV both show higher speed fluid forming four branches in the wake extending from the trailing edge top and bottom corners, helping to validate the accuracy of the numerical results.

Dominant Structures

The proper orthogonal decomposition (POD) is used to examine the temporal evolution of the wake at $Re = 2000$. The iso-surfaces in Figure 9 are the streamwise component of the four most energetic POD modes. The faster movement of vortices on the wake centerline relative to its edges resulted in a deformation of the structures shed from the panel trailing edge. The first and second modes capture the wake splitting (2P mode) as previously seen for higher oscillating frequencies for rectangular panels (Buchholz & Smits, 2006; Şentürk & Smits, 2016). The split was less evident in Modes 3 and 4. The wavelength of the second mode pair (Figure 7b) was half of the first mode, while the wavelength of Modes 3 and 4 were half of Modes 1 and 2,

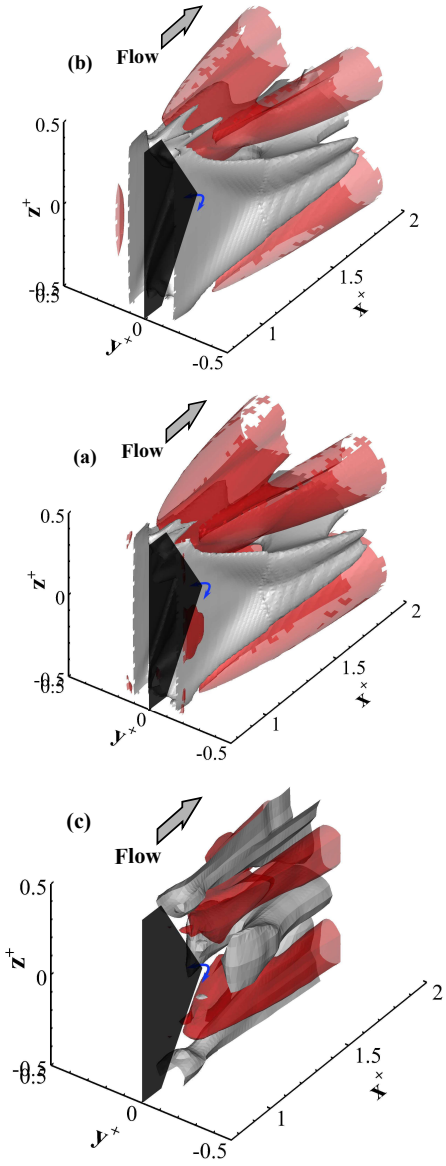

Figure 8: Iso-surface of $\overline{u^\star} = 0.93$ (gray) and 1.03 (red) for a thin convex panel at (a) $Re = 2000$ and (b) 10,000, compared with the (c) experimental results at $Re = 6000$ (Van Buren *et al.*, 2016).

respectively. Moreover, Mode 2 appeared to be more significantly influenced by the edges relative to Mode 1.

All four modes in Figure 9 exhibit an almost perfect symmetry on the $xy-$plane, while on the $xz-$plane the first mode was anti-symmetric and the second was symmetric. A similar alternation continues for the higher modes.

CONCLUSIONS

The wake of a simple oscillating flat panel was evaluated using a new Immersed Boundary Method incorporated into DNS at $Re = 2000$ and $10,000$. The *foam-extend 3.2*, which is an extension to OpenFOAM, was used to carry out these simulations. Following the initial verification of the solver capabilities, the wake characteristics were evaluated to determine the implications of the trailing edge, the effect of Reynolds number and the dominant features of wake structures using POD.

The higher efficiency and larger thrust generation by the triangular panel, compared to the square panel, were attributed to a smaller wake, shorter recirculation region, and

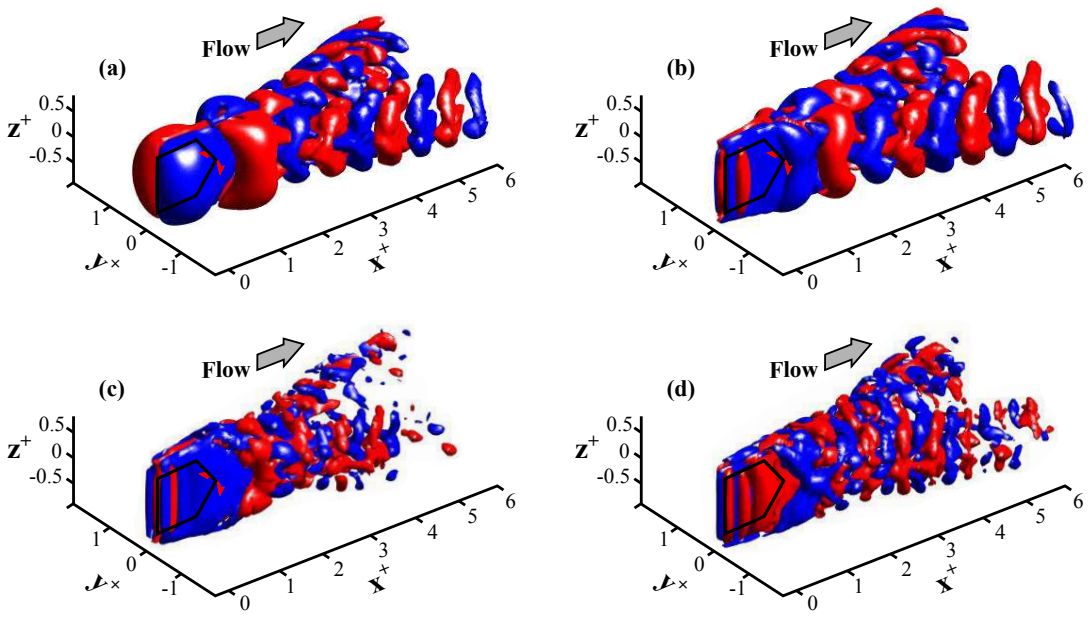

Figure 9: Isosurface of streamwise component (blue: 10% of minimum value, and red: 10% of maximum value) of the four most energetic POD modes at $Re = 2000$. (a) Mode 1, (b) Mode 2, (c) Mode 3, and (d) Mode 4.

larger velocity at the sharp edges of the panel. The smaller vortex distortion on the plane that is perpendicular to the axis of pitching, and larger distortion on the plane parallel to the panel surfaces coincided with the higher efficiency and thrust.

The effect of *Re* on the time-averaged wake characteristics was significant between $Re = 2000$ and $10,000$. The higher *Re* shortened the base region while forming a smaller low velocity region on the panel. The latter restricted low velocity fluid to close vicinity of the leading edge and resulted in lower drag, and thus, higher thrust and efficiency.

The POD modes confirmed split of the wake to two separate streets at the lower *Re* of 2000. Moreover, the distortion of shed off structures was suspended shortly after the initial detachment, which was recognized by the downstream structures retaining the shape of the trailing edge. The structures in all POD modes were relatively symmetric or anti-symmetric.

ACKNOWLEDGMENTS We gratefully acknowledge the support of the National Science and Engineering Research Council of Canada (NSERC), and the U.S. Office of Naval Research under MURI grant number N00014-14-1-0533 (program director Dr. Robert Brizzolara).

REFERENCES

Blondeaux, P., Fornarelli, F. & Guglielmini, L. 2005 Numerical experiments on flapping foils mimicking fish-like locomotion. *Physics of Fluids* **17** (11), 113601.

Buchholz, J. H. J. & Smits, A. J. 2006 On the evolution of the wake structure produced by a low-aspect-ratio pitching panel. *Journal of Fluid Mechanics* **546**, 433–443.

Şentürk, U., Brunner, D., Jasak, H., Herzog, N., Rowley, C. W. & Smits, A. J. 2016 Benchmark simulations of flow past rigid bodies using an open-source, sharp interface immersed boundary method. *Progress in Computational Fluid Dynamics* p. under review.

Şentürk, U. & Smits, A. J. 2016 Numerical simulations of the flow around a square pitching panel. *Journal of Fluids and Structures* p. under review.

Green, M. A., Rowley, C. W. & Smits, A. J. 2011 The unsteady three-dimensional wake produced by a trapezoidal pitching panel. *J. of Fluid Mechanics* **685**, 117–145.

Green, M. A. & Smits, A. J. 2008 Effects of three-dimensionality on thrust production by a pitching panel. *Journal of fluid mechanics* **615**, 211–220.

Iaccarino, G. & Verzicco, R. 2003 Immersed boundary technique for turbulent flow simulations. *Applied Mechanics Reviews* **56** (3), 331–347.

Jantzen, R. T., Taira, K., Granlund, K. O. & Ol, M. V. 2014 Vortex dynamics around pitching plates. *Physics of Fluids* **26** (5).

Jasak, H. 1996 Error analysis and estimation for the finite volume method with applications to fluid flows. PhD thesis, Imperial College London, UK.

Jasak, H., Rigler, D. & Tuković, Ž. 2014 Design and implementation of Immersed Boundary Method with discrete forcing approach for boundary conditions. In *11th World Congress on Computational Mechanics*, pp. 5319–5332.

Jeong, J. & Hussain, F. 1995 On the identification of a vortex. *Journal of Fluid Mechanics* **285**, 69–94.

Lundquist, K. A., Chow, F. K. & Lundquist, J. K. 2009 An Immersed Boundary Method for the Weather Research and Forecasting Model. *Monthly Weather Review* **138** (3), 796–817.

Mittal, R. & Iaccarino, G. 2005 Immersed Boundary Methods. *Ann. Rev. of Fluid Mechanics* **37** (1), 239–261.

Sambiley, V. 1990 Interrelationships between swimming speed, caudal fin aspect ratio and body length of fishes. *Fishbyte* **8**, 16–20.

Sumich, J. L. & Morrissey, J. F. 2004 *Introduction to the Biology of Marine Life*. Jones & Bartlett Learning.

Taira, Kunihiko & Colonius, Tim 2009 Three-dimensional flows around low-aspect-ratio flat-plate wings at low Reynolds numbers. *Journal of Fluid Mechanics* **623**, 187–207.

Triantafyllou, M., Triantafyllou, G. & Gopalkrishnan, R. 1991 Wake mechanics for thrust generation in oscillating foils. *Physics of Fluids A: Fluid Dynamics* **3** (12), 2835–2837.

Tuković, Ž. & Jasak, H. 2012 A moving mesh finite volume interface tracking method for surface tension dominated interfacial fluid flow. *Computers & Fluids* (55), 70–84.

Van Buren, T., Floryan, D., Brunner, D., Şentürk, U. & Smits, A.J. 2016 Impact of trailing edge shape on the wake and propulsive performance of pitching panels. *Physical Rev. Fluids* .